DALTON
FULL PAPER

Stabilization of copper(III) complexes by substituted oxamate ligands

Beatriz Cervera,[a] José L. Sanz,[a] María J. Ibáñez,[a] Gema Vila,[a] Francesc LLoret,[a] Miguel Julve,*[,a] Rafael Ruiz,[b] Xavier Ottenwaelder,[b] Ally Aukauloo,[b] Sandrine Poussereau,[b] Yves Journaux *[,b] and M. Carmen Muñoz[c]

[a] *Departament de Química Inorgànica, Universitat de València, Dr. Moliner 50, 46100 Burjassot, València, Spain*
[b] *Laboratoire de Chimie Inorganique, URA 420, CNRS, Université de Paris-Sud, 91405 Orsay, France*
[c] *Departamento de Física Aplicada, Universidad Politécnica de València, Camino de Vera s/n, 46071 València, Spain*

A new series of monomeric copper(II) complexes of the related substituted oxamate ligands *N*,*N*′-naphthalene-1,8-diylbis(oxamate) (L^2) and *N*,*N*′-trimethylenebis(oxamate) (L^3) have been synthesized. The molecular structures of $[NBu_4]_2[CuL^2]$ and $[PPh_4]_2[CuL^3]\cdot 2H_2O$ have been determined by single-crystal X-ray analysis. The structure of the previously reported complex $[PPh_4]_2[CuL^1]$, where L^1 is the parent *o*-phenylenebis(oxamate), has been also determined. These are mononuclear four-co-ordinate copper(II) complexes with the metal center in a more or less distorted square-planar environment formed by the two amido nitrogen and two carboxylate oxygen atoms from the two oxamato groups of each tetradentate chelating ligand. The bond lengths at the metal atom are similar for all three complexes, the Cu–N bond distances (1.89–1.93 Å) being shorter than the Cu–O ones (1.93–1.97 Å). The bond angles around the metal are different from one complex to the other. They are closer to 90°, corresponding to the ideal square-planar geometry, for the copper(II)–L^2 and –L^3 complexes as a result of the alternating 5-6-5-membered chelate ring system afforded by L^2 and L^3, respectively. The values of the Cu^{III}–Cu^{II} redox potential in acetonitrile for this family of complexes range from 0.41 to 0.27 V (*vs.* saturated calomel electrode, 25 °C and 0.1 mol dm^{-3} NEt_4ClO_4 as supporting electrolyte), the redox process being only reversible for the copper(II)–L^3 species. The stabilization of the trivalent oxidation state of copper in this complex is attributed to the stronger basicity of the aliphatic amido nitrogens with respect to that of the aromatic amido ones. The trend in formal potential along this series is mainly controlled by the size of the chelate rings around the metal ion.

An investigation to assess the possible use of substituted oxamate and oxamide ligands in the stabilization of unusual high-oxidation-state transition-metal ions has been initiated by us recently.[1] The preliminary studies with copper and *N*,*N*′-*o*-phenylenebis(oxamate), hereafter noted L^1, revealed that its copper(II) complex $[CuL^1]^{2-}$ oxidizes at a relatively low potential (+0.41 V *vs.* saturated calomel electrode) leading to formation of the corresponding copper(III) complex $[CuL^1]^-$. At the time we had not explicitly considered the potential redox-non-innocent character of this ligand containing an aromatic benzene group. In fact, several forms of the complex $[CuL^1]^-$ are possible in which the formal oxidation state of the metal center is different, *e.g.* **A**–**C**. Furthermore, copper(III) being a rare oxidation state,[1,2] one can question if the oxidized metal–L^1 species is correctly formulated as a copper(III) complex **B** or is best described as a ligand-oxidized copper(II) species **C**. In order to give a clear-cut answer to the uncertainty regarding the metal *versus* ligand oxidation, we have used a strategy which consists of following the shifts in the formal potentials in a series of related complexes upon replacing potentially non-innocent ligand fragments by innocent ones.[2e]

In this paper we explore the capacity of a specific family of substituted oxamate ligands derived from the parent *N*,*N*′-*o*-phenylenebis(oxamate) (L^1), namely its naphthalene-1,8-diyl (L^2) and trimethylene (L^3) derivatives, in the stabilization of copper(III) complexes; L^2, which is obviously a potentially non-innocent ligand, has its innocent counterpart in L^3. The trend displayed by the formal potentials as the aromatic groups are replaced by aliphatic ones along this series supports metal-centered oxidation of each copper(II) complex. The crystal and molecular structures of the copper(II) complexes with L^1, L^2 and L^3 ligands are also reported. This structural information allows us to establish the main factors which account for the differences in the electrochemical behavior for each copper compound, particularly the match between the metal cation and the cavity dimensions of each tetraanionic chelating ligand or the shape it adopts after co-ordination.

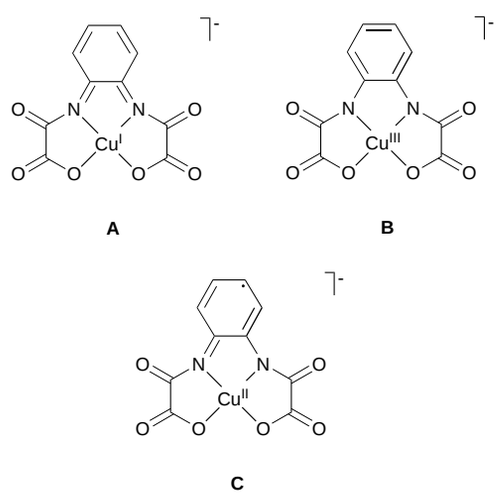

A **B** **C**

Experimental

Materials

All chemicals were of reagent-grade quality from commercial sources and used as received, except those for electrochemical

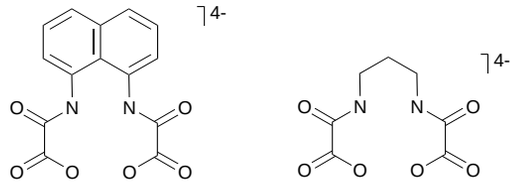

L^2 L^3

measurements. The NEt_4ClO_4 salt was recrystallized twice from acetone–diethyl ether and dried at 80 °C under vacuum. Acetonitrile was purified by distillation from calcium hydride on to activated 3 Å molecular sieves and stored under argon. The diethyl ester of *N*,*N*′-*o*-phenylenebis(oxamic acid) was prepared from ethyloxalyl chloride and *o*-phenylenediamine by literature methods.[3]

Preparations

H_4L^2. The diethyl ester of H_4L^2 was prepared in an analogous way to that reported for H_4L^1: naphthalene-1,8-diamine (4.75 g, 30 mmol) dissolved in tetrahydrofuran (100 cm^3) was added dropwise *via* a dropping funnel to a tetrahydrofuran solution (150 cm^3) of ethyloxalyl chloride (7 cm^3, 60 mmol) at room temperature with vigorous stirring. The resulting mixture was refluxed for 0.5 h and then filtered to remove the brown solid residue. The filtered solution was concentrated on a rotatory evaporator and the solvent volume reduced to 50 cm^3. Slow addition of diethyl ether resulted in the formation of a brick-red polycrystalline powder which was filtered off and dried under vacuum. Upon standing a second crop separated which was also collected and dried (90%). $\tilde{\nu}_{max}/cm^{-1}$ (KBr) 3360s and 3290s (NH) and 1730 (sh) and 1705vs (CO). $\delta_H[(CD_3)_2SO]$ 1.33 (6 H, t, 2 CH_3), 4.30 (4 H, q, 2 CH_2O), 7.56 (2 H, dd, *p*-H of $C_{10}H_6$), 7.60 (2 H, t, *m*-H of $C_{10}H_6$), 7.96 (2 H, dd, *o*-H of $C_{10}H_6$) and 10.75 (2 H, s, 2 NH).

H_4L^3. The diethyl ester of H_4L^3 was prepared following a procedure adapted from that employed for H_4L^2: a mixture of trimethylenediamine (2.5 cm^3, 30 mmol) and triethylamine (8.4 cm^3, 60 mmol) in tetrahydrofuran (100 cm^3) was added dropwise *via* a dropping funnel to a tetrahydrofuran solution (150 cm^3) of ethyloxalyl chloride (7 cm^3, 60 mmol) with vigorous stirring on an ice-bath. The resulting mixture was stirred for 0.5 h at room temperature and then filtered to eliminate the white precipitate of NEt_3HCl. The solvent was removed on a rotatory evaporator and the remaining oil treated with diethyl ether to give a white solid which was filtered off and dried under vacuum (75%). $\tilde{\nu}_{max}/cm^{-1}$ (KBr) 3305s (NH) and 1755s and 1680vs (CO). $\delta_H[(CD_3)_2SO]$ 1.25 (6 H, t, 2 CH_3), 1.63 (2 H, q, CH_2), 3.11 (4 H, t, 2 CH_2N), 4.20 (4 H, q, 2 CH_2O) and 8.91 (2 H, t, 2 NH).

$[PPh_4]_2[CuL^1]$ 1. Well shaped violet prismatic crystals of complex **1** suitable for X-ray analysis were obtained by slow evaporation of a water–methanol solution of its monohydrate form prepared by metathesis of the sodium salt $Na_2[CuL^1]\cdot 3H_2O$ with PPh_4Cl in water as described previously.[1]

$Na_2[CuL^2]\cdot 2H_2O$ 2. The copper(II) complex **2** was synthesized by a procedure analogous to that reported previously for $Na_2[CuL^1]\cdot 3H_2O$:[3] to a suspension of the diethyl ester of H_4L^2 (1.80 g, 5 mmol) in water (250 cm^3) was added an aqueous solution (25 cm^3) of NaOH (0.80 g, 20 mmol). The resulting mixture was stirred at 60 °C for 15 min until complete dissolution. An aqueous solution (50 cm^3) of $Cu(NO_3)_2\cdot 3H_2O$ (1.20 g, 5 mmol) was then added dropwise with stirring. The dark green solution was filtered to eliminate solid particles, reduced to approximately one half of the initial volume on a rotatory evaporator when a solid began to appear. The green powdered precipitate was filtered off, washed with ethanol and ether, and air-dried.

$[NEt_4]_2[CuL^2]\cdot 2H_2O$ 3. To a suspension of the diethyl ester of H_4L^2 (1.80 g, 5 mmol) in methanol (100 cm^3) was added a 25% methanolic solution (13 cm^3) of NEt_4OH (20 mmol). The resulting mixture was stirred at 60 °C for 15 min. A methanolic solution (50 cm^3) of $Cu(ClO_4)_2\cdot 6H_2O$ (1.85 g, 5 mmol) was then added dropwise with stirring. The resulting dark purple solution was filtered and the solvent removed on a rotatory evaporator. The product obtained was dissolved in absolute ethanol (300 cm^3) and the purple solution filtered to eliminate solid NEt_4ClO_4. The solvent was removed again on a rotatory evaporator to give a purple hygroscopic product which was recovered with acetone, filtered off and dried under vacuum.

$[NBu_4]_2[CuL^2]$ 4. The copper(II) complex **4** was prepared by a similar procedure to that reported for $[NBu_4]_2[CuL^1]$:[3] a 1.0 mol dm^{-3} methanolic solution (20 cm^3) of NBu_4OH (20 mmol) was added to an aqueous suspension (75 cm^3) of the diethyl ester of H_4L^2 (1.80 g, 5 mmol). The mixture was stirred at 60 °C for 15 min. An aqueous solution (50 cm^3) of $CuCl_2\cdot 2H_2O$ (0.85 g, 5 mmol) was then added dropwise with stirring. The dark brown solution was filtered, reduced to 50 cm^3 on a rotatory evaporator, and extracted with dichloromethane (500 cm^3). The dichloromethane phase became intensely colored while the aqueous one turned colorless. The organic phase was separated from the mixture, washed twice with water and dried over $MgSO_4$. The deep purple solution was allowed to evaporate, and the resulting product treated with acetone to leave a somewhat hygroscopic purple solid which was filtered off and dried under vacuum. Recrystallization from nitromethane afforded purple plate-like crystals of **4** which were suitable for X-ray analysis.

$Na_2[CuL^3]\cdot 6H_2O$ 5. The copper(II) complex **5** was synthesized by following a different procedure to that reported previously:† an aqueous solution (25 cm^3) of NaOH (1.00 g, 25 mmol) was added to a suspension of the diethyl ester of H_4L^3 (1.37 g, 5 mmol) in water (50 cm^3). After stirring for 15 min at room temperature, an aqueous solution (25 cm^3) of $Cu(NO_3)_2\cdot 3H_2O$ (1.20 g, 5 mmol) was added dropwise. The deep blue solution was then filtered to eliminate the solid particles and the solvent volume was reduced to 25 cm^3 on a rotatory evaporator. Slow addition of absolute ethanol to the mother-liquor gave a red microcrystalline solid which was filtered off and air-dried. Upon standing a second crop separated which was also collected and dried.

$[NMe_4]_2[CuL^3]\cdot H_2O$ 6. A 25% methanolic solution (10 cm^3) of NMe_4OH (25 mmol) was added to a suspension of the

† The synthesis from the reaction of the *N*,*N*′-trimethylenebis(oxamide) (H_4L^4) with copper(II) in an aqueous basic medium was reported some time ago.[4] This procedure, however, is often accompanied by side reactions and low yields (50%), and moreover it is a rather tedious route due to the evolution of NH_3 during the course of the hydrolytic reaction. It is well documented that hydrolysis of primary amide groups proceeds slowly in alkaline solution, but very fast in the presence of the copper(II) ion. In contrast, nickel(II) ion does not cause hydrolysis of the oxamide, thus allowing the preparation of the corresponding nickel(II) oxamidate complex $Na_2[NiL^4]\cdot 4H_2O$,[4] where both the primary and the secondary amide groups are co-ordinated *via* their deprotonated nitrogen atoms. The infrared spectrum of $Na_2[NiL^4]\cdot 4H_2O$ shows a sharp band at 3293 cm^{-1} assignable to ν(NH) of the primary amides, which is not observed for $Na_2[CuL^3]\cdot 6H_2O$. From this peculiar difference in the infrared spectra between the nickel(II) and copper(II) complexes it was concluded that the ligand complement from the copper(II) compound obtained by reaction of copper(II) with the oxamide ligand in water was effectively hydrolyzed, even when no structural evidence was available at that time.[4]

diethyl ester of H_4L^3 (1.37 g, 5 mmol) in methanol (100 cm^3). The resulting mixture was stirred at 60 °C for 15 min. A methanolic solution (50 cm^3) of $Cu(ClO_4)_2 \cdot 6H_2O$ (1.85 g, 5 mmol) was then added dropwise with stirring. The deep blue solution was filtered to remove solid NMe_4ClO_4, and reduced to *ca.* 10 cm^3 on a rotatory evaporator. The mixture was treated successively with ether and acetone to give a red hygroscopic solid which was recovered with acetonitrile, filtered off and dried under vacuum.

$[PPh_4]_2[CuL^3] \cdot 2H_2O$ 7. The sodium salt **5** (1.73 g, 4 mmol) and $AgNO_3$ (1.36 g, 8 mmol) in water (50 cm^3) afforded $Ag_2[CuL^3]$ which precipitated in almost quantitative yield. The product was filtered off and suspended in water (50 cm^3). Addition of solid PPh_4Cl (3.00 g, 8 mmol) followed by gentle warming for 0.5 h resulted in a white precipitate of AgCl and a deep blue solution. The reaction mixture was then filtered, and the solvent removed on a rotatory evaporator to yield a reddish purple solid. Redissolution in a water–methanol mixture afforded well shaped red prisms of complex **7** suitable for X-ray analysis after slow evaporation at room temperature. The isolation of the tetraphenylphosphonium salt by the usual method which consists of treating the corresponding sodium salt with an excess of PPh_4Cl in water[1] is precluded in this case because of its high solubility in this medium.

Analytical and general physical characterization data for the complexes **1**–**7** are listed in Table 1.

Physical techniques

Proton NMR spectra were recorded at 250 MHz on a Bruker AC 250 spectrometer. Chemical shifts are reported in δ (ppm) *vs.* $SiMe_4$ with the deuteriated dimethyl sulfoxide (dmso) solvent proton residuals as internal standard. The ESR solution spectra were recorded on a Bruker ER 200 D spectrometer at X-band at 140 K, IR spectra on a Perkin-Elmer 882 spectrophotometer as KBr pellets and UV/VIS solution spectra on a Perkin-Elmer Lambda 9 spectrophotometer. Elemental analyses (C, H, N) were performed by the Microanalytical Service of the Universidad Autónoma de Madrid (Spain).

Cyclic voltammetry and controlled-potential electrolysis were performed using an EGG PAR model M273 scanning potentiostat operating at a scan rate of 10–1000 mV s^{-1}. The cyclic voltammetric studies were carried out in acetonitrile using 0.1 mol dm^{-3} NEt_4ClO_4 as supporting electrolyte, and 1.0 mmol dm^{-3} of complexes **1**, **4** and **7**. The tetraphenylphosphonium salt **1** gave identical results to that reported previously for the monohydrate form under the same conditions (*i.e.* 50–200 mV s^{-1}).[1] The working electrode was a glassy carbon disk (0.32 cm^2) which was polished with 1 μm polishing powder, washed with absolute ethanol and air-dried. The reference electrode was Ag–$AgClO_4$ separated from the test solution by a salt bridge containing the solvent/supporting electrolyte, with platinum as auxiliary electrode. The experiments were performed in a standard electrochemical cell under an inert atmosphere at 25 °C. The potential range investigated was from −1.00 to 1.80 V. All formal potentials were taken as the anodic peak potentials measured at a scan rate of 100 mV s^{-1} and are referred to the saturated calomel electrode (SCE), which was consistently measured as −0.26 V *vs.* the $AgClO_4$–Ag electrode. The coulometric studies were carried out in acetonitrile using 0.2 mol dm^{-3} NBu_4PF_6 as supporting electrolyte and 1.0 mmol dm^{-3} of complex **7**. The experiments were performed with a glassy carbon gauze electrode in a standard electrolysis cell under an inert atmosphere at −40 °C. The oxidized species was generated at 0.50 V *vs.* SCE.

Crystallography

Crystal data and data collection parameters. Crystals of dimensions 0.1 × 0.2 × 0.1 (complex **1**), 0.05 × 0.1 × 0.1 (**4**) and 0.2 × 0.1 × 0.1 mm (**7**) were mounted on an Enraf-Nonius CAD-4 diffractometer and used for data collection. Intensity data were collected at 293 K by using graphite-monochromated Mo-Kα radiation (λ = 0.710 73 Å) with the ω–2θ scan method. The unit-cell parameters were determined from least-squares refinements on the setting angles from 25 centered reflections in the range $12 < \theta < 20°$. No significant fluctuations were observed in the intensities of three standard reflections monitored periodically throughout data collection. Intensity data were corrected for Lorentz-polarization and absorption corrections. Of the 3251 (**1**), 3214 (**4**) and 3296 (**7**) measured independent reflections, 2828 (**1**), 1500 (**4**) and 2786 (**7**) were unique with $I \geqslant 2\sigma(I)$ and used for the structure refinements. Crystal parameters and structure refinements are summarized in Table 2.

Structure solution and refinement. The structures were solved by Patterson methods and refined by the full-matrix least-squares method on F^2 for 623 (**1**), 261 (**4**) and 615 (**7**) refined parameters. The computations were performed with the programs SHELXS 86 and SHELX 93.[5] Non-hydrogen atoms were treated anisotropically. The hydrogen atoms were located from a difference synthesis and refined with an overall isotropic thermal parameter, except those from the two crystallization water molecules of **3** which were neither found nor calculated. The final full-matrix least-squares refinements minimizing $\Sigma w(|F_o| - |F_c|)^2$ converged at the values of R and R' listed in Table 2. Values of f, f' and f'' were taken from ref. 6. The residual maxima and minima in the final Fourier-difference maps were 0.179 and −0.372 (**1**), 0.224 and −0.201 (**4**) and 0.309 and −0.396 e $Å^{-3}$ (**7**). The molecular plots were drawn with the ORTEP program.[7] Selected bond distances and angles for complexes **1**, **4** and **7** are listed in Tables 3, 4 and 5, respectively.

CCDC reference number 186/834.

Results and Discussion

Structures

Complex 1. The structure of $[PPh_4]_2[CuL^1]$ **1** consists of discrete monomeric copper complex anions, $[CuL^1]^{2-}$, and tetraphenylphosphonium cations. A perspective view of the anion with the atom-numbering scheme is depicted in Fig. 1 (top). The anion entity has an almost planar structure [maximum deviations from the mean molecular plane of 0.224 and 0.267 Å for O(1) and O(4), respectively], as illustrated in Fig. 1 (bottom).

The copper atom is co-ordinated to the two deprotonated amido nitrogens and two carboxylate oxygens of the chelating ligand in a distorted square-planar geometry [deviations from the N(1)N(2)O(3)O(6) mean plane are ±0.035 Å for N(1) and N(2) and ±0.028 Å for O(3) and O(6), with the metal atom being 0.007 Å out of this mean plane]. The ligand L^1 adopts a tetradentate co-ordination mode forming three five-membered chelate rings around the metal ion. This pattern of 5-5-5 fused chelate rings imposes a severe distortion of the metal environment from the ideal square plane. The rather tight fit on the N(1)–Cu–N(2) angle (83.3°) causes an opening of the O(3)–Cu–O(6) angle (106.1°), whereas the bite angles of the two oxamato chelating groups are closer to 90° [86.5 and 84.1° for N(1)–Cu–O(3) and N(2)–Cu–O(6), respectively]. This is a unique feature of planar complexes with the 5-5-5 ring system: three of the bond angles at the metal are roughly equal and the fourth one, being less constrained, is appreciably larger. The average Cu–N (amide) bond length (1.910 Å) is significantly shorter than the average Cu–O (carboxylate) one (1.945 Å) in agreement with the greater basicity of the former, as previously found for the copper(II) complex $[Ru(bipy)_3][CuL^1] \cdot 9H_2O$ (bipy = 2,2′-bipyridine).[8] All these features result in the formation of a trapezoidal N_2O_2 co-ordination center around copper, as illustrated in Fig. 4(*a*), with the O···O distance being

Table 1 Analytical[a] and physical data for the copper(II) complexes **1**–**7**

Complex	Color	$\tilde{\nu}$(CO)[b]/cm^{-1}	Yield (%)	Analysis (%) C	H	N
1 $[PPh_4]_2[CuL^1]$	Violet	1645s, 1620vs	90	70.1 (70.3)	4.4 (4.4)	2.7 (2.8)
2 $Na_2[CuL^2]\cdot 2H_2O$	Green	1655s (sh), 1625vs	90	38.4 (37.9)	2.0 (2.3)	6.7 (6.3)
3 $[NEt_4]_2[CuL^2]\cdot 2H_2O$	Purple	1645vs (br)	85	55.0 (54.8)	7.5 (7.6)	8.15 (8.5)
4 $[NBu_4]_2[CuL^2]$	Purple	1645vs	75	65.5 (65.3)	9.5 (9.2)	6.7 (6.6)
5 $Na_2[CuL^3]\cdot 6H_2O$	Red	1640vs, 1625s (sh)	90	19.6 (19.5)	4.1 (4.2)	6.45 (6.5)
6 $[NMe_4]_2[CuL^3]\cdot H_2O$	Red	1635vs, 1605vs	80	42.0 (40.6)	7.3 (7.3)	13.15 (12.6)
7 $[PPh_4]_2[CuL^3]\cdot 2H_2O$	Red	1630vs, 1604vs	85	66.2 (66.6)	5.5 (5.1)	2.7 (2.8)

[a] Required values are given in parentheses. [b] In KBr.

Table 2 Summary of crystal data for $[PPh_4]_2[CuL^1]$ **1**, $[NBu_4]_2[CuL^2]$ **4** and $[PPh_4]_2[CuL^3]\cdot 2H_2O$ **7**

	1	**4**	**7**
Formula	$C_{58}H_{44}CuN_2O_6P_2$	$C_{46}H_{78}CuN_4O_6$	$C_{55}H_{50}CuN_2O_8P_2$
M	990.43	846.66	992.45
Crystal system	Monoclinic	Monoclinic	Orthorhombic
Space group	$P2_1$	$C2/c$	$Pna2_1$
a/Å	10.542(5)	18.835(3)	34.688(5)
b/Å	17.028(5)	17.424(3)	11.591(2)
c/Å	13.392(4)	14.977(2)	11.890(2)
β/°	97.38(3)	91.063(11)	
U/Å^3	2384.2(15)	4914.3(12)	4780.8(14)
Z	2	4	4
D_c/g cm^{-3}	1.380	1.144	1.379
F(000)	1026	1836	2068
μ(Mo-Kα)/cm^{-1}	0.581	0.451	0.583
θ Range/°	2.0–22.5	2.0–22.5	2.0–22.5
R[a]	0.035	0.072	0.044
R'[b]	0.085	0.110	0.104
w[c]	$1/[\sigma^2(F_o^2) + (0.0770P)^2 + 10.5233P]$	$1/[\sigma^2(F_o^2) + (0.0369P)^2]$	$1/[\sigma^2(F_o^2) + (0.0498P)^2 + 8.7953P]$

[a] $\Sigma(|F_o| - |F_c|)/\Sigma(|F_o|)$. [b] $[\Sigma(|F_o| - |F_c|)^2/\Sigma wF_o^2]^{\frac{1}{2}}$. [c] $P = (F_o^2 + 2F_c^2)/3$.

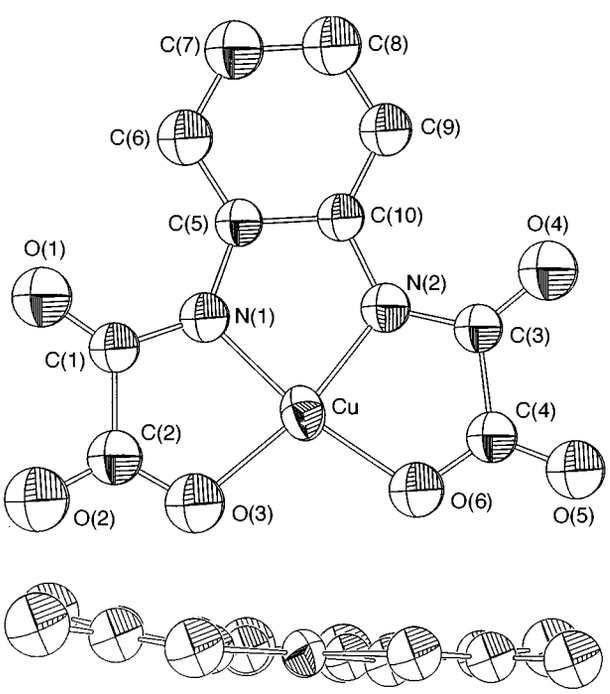

Fig. 1 Perspective view of the anionic mononuclear unit of complex **1** (top, viewed from above, with the atom-numbering scheme; bottom, side view). Thermal ellipsoids are drawn at the 30% probability level; hydrogen atoms have been omitted for clarity

Table 3 Selected bond lengths (Å) and interbond angles (°) for complex **1** with estimated standard deviations (e.s.d.s) in parentheses

Copper environment			
Cu–N(1)	1.888(6)	Cu–O(3)	1.925(5)
Cu–N(2)	1.931(6)	Cu–O(6)	1.966(6)
N(1)–Cu–N(2)	83.3(3)	N(1)–Cu–O(3)	86.5(3)
N(1)–Cu–O(6)	167.4(3)	O(3)–Cu–O(6)	106.1(3)
N(2)–Cu–O(3)	169.5(3)	N(2)–Cu–O(6)	84.1(3)
Cu–N(1)–C(1)	114.5(6)	Cu–N(1)–C(5)	115.9(5)
Cu–O(3)–C(2)	111.6(5)	Cu–O(6)–C(4)	112.4(5)
Cu–N(2)–C(3)	115.7(6)	Cu–N(2)–C(10)	114.7(5)
L^1			
C(1)–O(1)	1.238(9)	C(2)–O(2)	1.219(10)
C(3)–O(4)	1.239(10)	C(4)–O(5)	1.218(10)
C(1)–N(1)	1.337(9)	C(2)–O(3)	1.304(10)
C(3)–N(2)	1.336(10)	C(4)–O(6)	1.291(10)
C(1)–C(2)	1.557(11)	C(5)–N(1)	1.405(10)
C(3)–C(4)	1.567(13)	C(10)–N(2)	1.403(9)
O(1)–C(1)–N(1)	127.6(8)	O(2)–C(2)–O(3)	124.0(8)
O(4)–C(3)–N(2)	128.3(8)	O(5)–C(4)–O(6)	123.4(9)
O(1)–C(1)–C(2)	121.6(7)	O(2)–C(2)–C(1)	119.7(8)
O(4)–C(3)–C(4)	121.8(7)	O(5)–C(4)–C(3)	119.6(9)
N(1)–C(1)–C(2)	110.7(7)	O(3)–C(2)–C(1)	116.2(7)
N(2)–C(3)–C(4)	109.9(7)	O(6)–C(4)–C(3)	117.0(7)
C(1)–N(1)–C(5)	128.7(7)	C(3)–N(2)–C(10)	128.8(7)
N(1)–C(5)–C(10)	113.1(7)	N(1)–C(5)–C(6)	127.3(7)
N(2)–C(10)–C(5)	112.9(7)	N(2)–C(10)–C(9)	128.3(7)

remarkably larger than that between the nitrogen atoms within the *o*-phenylenediamine unit.

Complex 4. The structure of $[NBu_4]_2[CuL^2]$ **4** is made up of discrete monomeric copper complex anions, $[CuL^2]^{2-}$, and tetrabutylammonium cations. A perspective view of the mononuclear anionic entity with the atom-numbering scheme is depicted in Fig. 2 (top). Interestingly, the copper atom lies on a two-fold axis which passes through the C(7)–C(8) bond, and consequently, the ligand L^2 presents a C_2 symmetry.

The co-ordination geometry of the copper atom is distorted

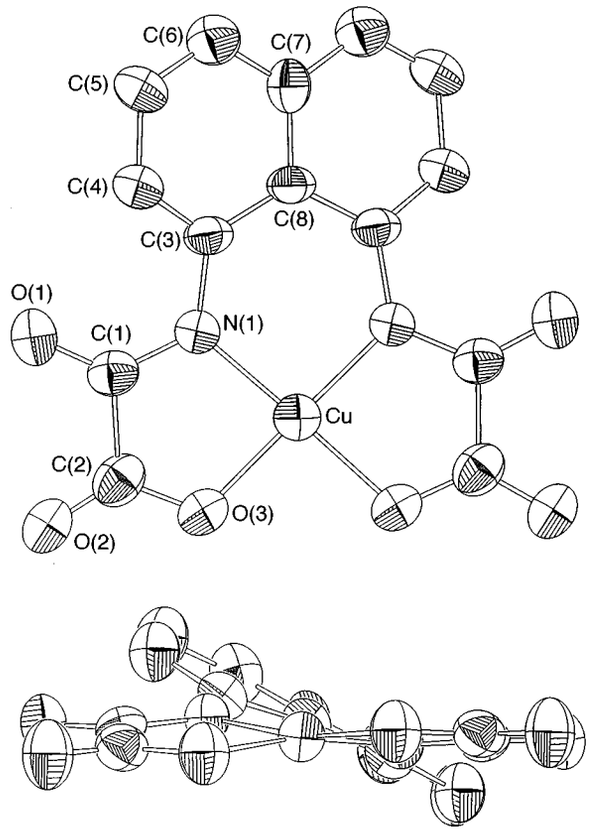

Fig. 2 Perspective view of the anionic mononuclear unit of complex **4**. Details as in Fig. 1

square planar, involving the two deprotonated amido nitrogen and two carboxylate oxygen atoms of the tetradentate ligand. The copper–nitrogen bond length (1.912 Å) is practically identical to that found in complex **1**, but the copper–oxygen one (1.925 Å) is somewhat shortened. The bond angles around copper are markedly different. They span the narrow range 86.7–95.6°, values which are close to 90° corresponding to the ideal square-planar geometry, as a result of the 5-6-5-membered chelate ring system imposed by the L^2 ligand. The formation of an approximately square N_2O_2 cavity is allowed here, as illustrated in Fig. 4(*b*), with the O···O distance being virtually identical to the N···N distance within the naphthalene-1,8-diamine unit. Although the four donor atoms are in good alignment with the copper center, the N_2O_2 co-ordination scheme deviates from planarity more markedly than in the case of **1**. So, whereas the N_2O_2 core in **1** is almost planar, that of **4** takes on a corrugated conformation [the deviations from the N(1)N(1^I)O(3)O(3^I) mean plane are ±0.177 Å for N(1) and N(1^I) and ±0.180 Å for O(3) and O(3^I), the metal atom belonging to the mean plane], thus resulting in a slight tetrahedral distortion of the copper(II) environment. This structural feature is unexpected since one would have predicted an even lower distortion from the ideal square-planar geometry due to the presence of the central six-membered chelate ring that would relieve the geometric constraints (relative to the five-membered pattern). In this sense, it is noteworthy that the entire L^2 skeleton, in contrast to that of L^1, is no longer planar, but exhibits a considerable twist because of the van der Waals repulsion between the amido oxygen atoms O(1) and O(1^I) and the aromatic hydrogens in the *ortho* positions from the naphthalene ring [the dihedral angle between the mean planes comprising the naphthalene fragment and the oxamato group is 26.8° *versus* 5.8 and 6.7° for the corresponding angles between the phenylene fragment and those of the oxamato groups in **1**]. This can be seen very nicely in Fig. 2 (bottom). Thus, the

Table 4 Selected bond lengths (Å) and interbond angles (°) for complex **4** with e.s.d.s in parentheses*

Copper environment			
Cu–N(1)	1.912(5)	Cu–O(3)	1.925(5)
N(1)–Cu–N(1^I)	95.6(4)	N(1)–Cu–O(3)	86.7(2)
N(1)–Cu–O(3^I)	169.3(2)	O(3)–Cu–O(3^I)	92.9(3)
Cu–N(1)–C(1)	112.4(5)	Cu–N(1)–C(3)	125.0(5)
Cu–O(3)–C(2)	113.0(5)		
L^2			
C(1)–O(1)	1.240(8)	C(2)–O(2)	1.213(8)
C(1)–N(1)	1.350(8)	C(2)–O(3)	1.298(8)
C(1)–C(2)	1.561(9)	C(3)–N(1)	1.411(8)
O(1)–C(1)–N(1)	128.7(7)	O(2)–C(2)–O(3)	125.8(8)
O(1)–C(1)–C(2)	118.2(8)	O(2)–C(2)–C(1)	119.4(9)
N(1)–C(1)–C(2)	113.0(8)	O(3)–C(2)–C(1)	114.8(8)
C(1)–N(1)–C(3)	122.6(6)	N(1)–C(3)–C(8)	121.3(7)
N(1)–C(3)–C(4)	120.4(7)	C(3)–C(8)–C(3^I)	125.0(9)

* Symmetry code: I $-x, y, \frac{1}{2} - z$.

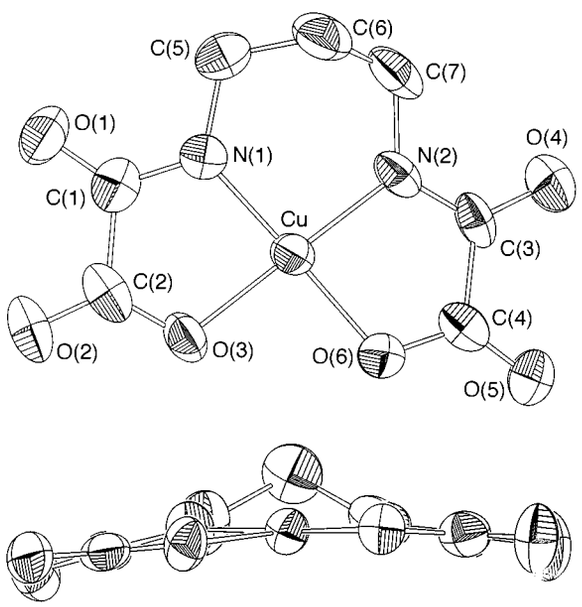

Fig. 3 Perspective view of the anionic mononuclear unit of complex **7**. Details as in Fig. 1

deviation of the ligand backbone from planarity is most likely responsible for the tetrahedral distortion of the copper co-ordination environment, as described above.

Complex 7. The structure of $[PPh_4]_2[CuL^3]\cdot 2H_2O$ **7** is composed of discrete monomeric copper complex anions, $[CuL^3]^{2-}$, tetraphenylphosphonium cations and water molecules of crystallization. A perspective view of the mononuclear anionic entity with the atom-numbering scheme is depicted in Fig. 3 (top). The anionic entities are linked by hydrogen bonds involving the O(2), O(4) and O(5) atoms from the oxamate groups and the water molecules of crystallization, thus leading to chains running along the *b* axis.

The co-ordination environment at the copper atom is nearly square planar, formed by the two deprotonated amido nitrogen and two carboxylate oxygen atoms of the tetradentate chelating ligand. Complex **7** shows great similarities with **4** in terms of both bond lengths (average Cu–N and Cu–O distances of 1.908 and 1.939 Å, respectively) and angles (84.2–96.4°) around copper. Moreover, the co-ordinated N_2O_2 set of atoms adopts a nearly square arrangement also in that case, as illustrated in Fig. 4(*c*). No changes were observed in the bond distances and

Table 5 Selected bond lengths (Å) and interbond angles (°) for complex **7** with e.s.d.s in parentheses*

Copper environment			
Cu–N(1)	1.913(7)	Cu–O(3)	1.947(6)
Cu–N(2)	1.903(7)	Cu–O(6)	1.931(6)
N(1)–Cu–N(2)	96.4(3)	N(1)–Cu–O(3)	84.2(3)
N(1)–Cu–O(6)	177.3(3)	O(3)–Cu–O(6)	94.2(3)
N(2)–Cu–O(3)	177.4(3)	N(2)–Cu–O(6)	85.3(3)
Cu–N(1)–C(1)	114.5(6)	Cu–N(1)–C(5)	126.1(6)
Cu–O(3)–C(2)	112.8(5)	Cu–O(6)–C(4)	113.0(6)
Cu–N(2)–C(3)	113.3(6)	Cu–N(2)–C(7)	125.6(6)
L^3			
C(1)–O(1)	1.254(10)	C(2)–O(2)	1.225(11)
C(3)–O(4)	1.250(11)	C(4)–O(5)	1.221(12)
C(1)–N(1)	1.307(11)	C(2)–O(3)	1.286(11)
C(3)–N(2)	1.333(12)	C(4)–O(6)	1.291(11)
C(1)–C(2)	1.544(13)	C(5)–N(1)	1.468(11)
C(3)–C(4)	1.534(13)	C(7)–N(2)	1.450(11)
O(1)–C(1)–N(1)	127.7(9)	O(2)–C(2)–O(3)	124.9(10)
O(4)–C(3)–N(2)	125.3(9)	O(5)–C(4)–O(6)	125.5(9)
O(1)–C(1)–C(2)	120.3(9)	O(2)–C(2)–C(1)	119.8(10)
O(4)–C(3)–C(4)	121.9(9)	O(5)–C(4)–C(3)	119.6(9)
N(1)–C(1)–C(2)	112.0(8)	O(3)–C(2)–C(1)	115.2(8)
N(2)–C(3)–C(4)	112.8(8)	O(6)–C(4)–C(3)	115.0(9)
C(1)–N(1)–C(5)	118.3(8)	C(3)–N(2)–C(7)	120.7(8)
N(1)–C(5)–C(6)	110.5(8)	N(2)–C(7)–C(6)	111.3(8)
C(5)–C(6)–C(7)	114.8(10)		
Hydrogen bonds			
O(4)···O(8)	2.756(14)	O(8)···O(7)	2.900(14)
O(7)···O(5)	2.813(14)	O(8)···O(2^I)	2.839(14)

* Symmetry code: I x, $1 + y$, z.

angles of the N_2O_2 core upon substitution of the rigid naphthalene-1,8-diyl by the more flexible trimethylene bridge, which serves to underline the common 5-6-5-membered chelate ring system pattern afforded by both ligands. In contrast with **4**, the planarity of the copper co-ordination environment is almost restored in **7** [deviations from the N(1)N(2)O(3)O(6) mean plane are ±0.040 Å for each atom, with the copper atom being only 0.004 Å out of this plane]. Moreover, the L^3 ligand is almost planar with the maximum deviation from planarity being observed at the C(6) atom of the trimethylene fragment (the distance from the mean molecular plane is 0.621 Å), as depicted in Fig. 3 (bottom).

Infrared and electronic spectra

The most relevant CO absorption bands for the copper(II) complexes **1**–**7** are listed in Table 1. Noticeable shifts are observed for the ν(CO) frequencies along this series of copper(II) complexes, reflecting the different extents of conjugation over the oxamato moieties for each species. In general, for the copper(II)–L^3 complexes the asymmetric C=O resonance frequency, corresponding to the average of the two vibrational modes ν_1(CO) and ν_7(CO),[1] is lower than that of the copper(II)–L^1 and –L^2 complexes. This observation is in agreement with a weakening of the double-bond character of the C=O amide bond and a more pronounced double-bond character of the C–N amide bond for the copper(II)–L^3 complex (see Tables 3–5). This phenomenon is explained by the larger inductive donating effect of the trimethylene group when compared to that of the aromatic phenylene or naphthalene groups which is reflected in an increased contribution of resonance form **II** to the main resonance form **I** for the amide function.

The electronic absorption spectra of the copper(II) complexes **1**, **4** and **7** in acetonitrile are shown in Fig. 5 [curves (*a*)–(*c*)]. Those of **1** and **4** show a similar pattern consisting of an intense band in the UV region, centered at 320 and 360 nm, respectively,

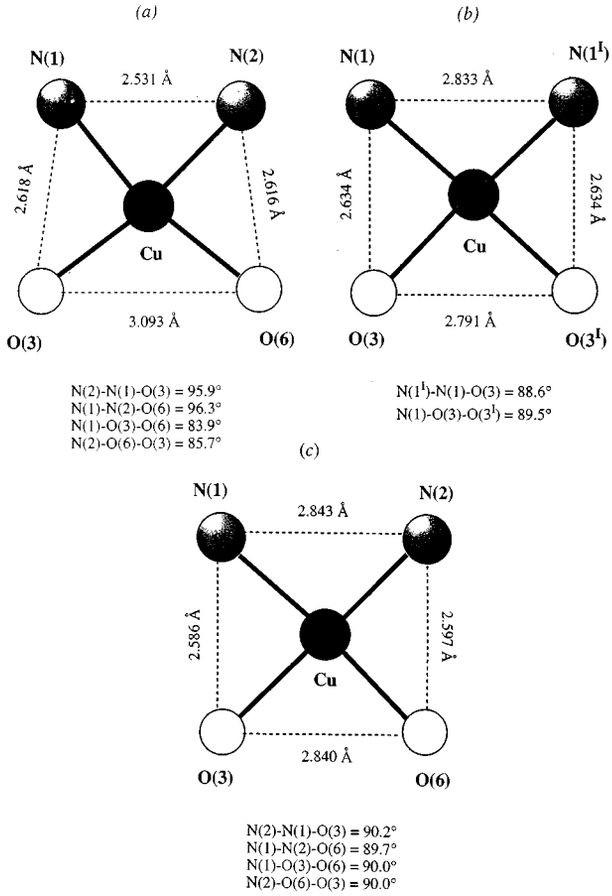

Fig. 4 Schematic view of the copper co-ordination environment of complexes **1** (*a*), **4** (*b*) and **7** (*c*) with relevant dimensions for the N_2O_2 metal-binding site

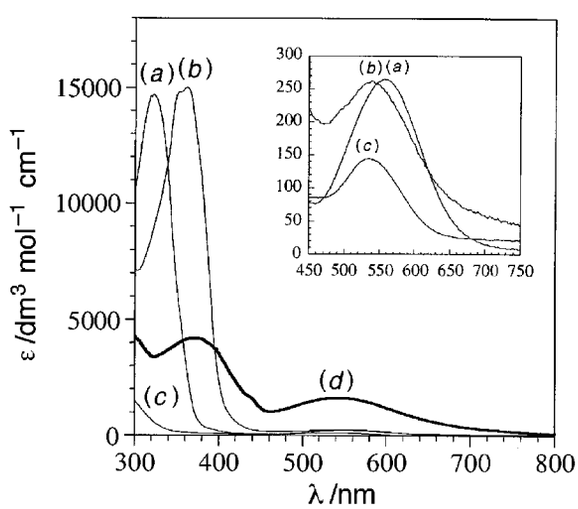

Fig. 5 Electronic absorption spectra of the copper(II) complexes **1** (*a*), **4** (*b*) and **7** (*c*) and of the electrochemically generated copper(III)–L^3 complex (*d*) in acetonitrile

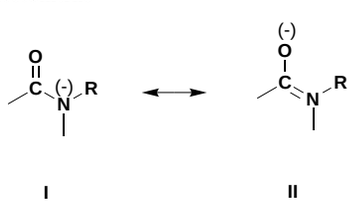

with a second less intense band in the visible region located at 560 and 540 nm, respectively. By contrast, **7** only shows a band of weak intensity in the visible zone located at 535 nm. The

high-energy band present in the spectra of **1** and **4**, but absent in that of **7**, is accordingly assigned to an intraligand π–π* transition within the aromatic ligands. The higher aromaticity of the naphthalene ring of L^2 relative to the phenylene ring of L^1 is presumably responsible for the bathochromic shift of the high-energy band of $[CuL^2]^{2-}$ compared to that of $[CuL^1]^{2-}$. Alternatively, this band may be attributed to a metal-to-ligand charge-transfer (MLCT) band from copper(II) to the aromatic ring. However, the presence of an intense band in the UV region of the spectra for the diethyl ester derivatives of H_4L^1 and H_4L^2 located at 255 and 310 nm, respectively, fits better with the former interpretation of an intraligand transition.

The visible band in the electronic absorption spectra of the copper(II) complexes **1**, **4** and **7** in acetonitrile solution, the location of which varies over the narrow range 560–535 nm depending upon the nature of the copper(II) complex, *i.e.* at 560, 540 and 535 nm, respectively [curves (*a*)–(*c*) in the insert of Fig. 5], is the characteristic d–d transition band of Cu^{II} with a d^9 electronic configuration in a square-planar environment.‡ This single absorption band actually is the envelope of three d–d transitions (*i.e.* $^2B_{1g} \longrightarrow {}^2A_{1g}$, $^2B_{1g} \longrightarrow {}^2B_{2g}$ and $^2B_{1g} \longrightarrow {}^2E_{1g}$ in ideal D_{4h} symmetry).[1] If the relative positions and intensities of these three transitions remain constant, the position of the maximum for the band envelope is a measure of the ligand-field strength afforded by each ligand and, hence, indicative of the crystal-field stabilization energy (CFSE). So, the significant red shift observed in the visible absorption maxima of both $[CuL^2]^{2-}$ and $[CuL^3]^{2-}$ relative to $[CuL^1]^{2-}$, in spite of the presence of the same CuN_2O_2 chromophote, indicates the stronger ligand field associated with the six- compared to the five-membered chelate rings. Actually, this ligand-field effect is explained in terms of the stronger metal–ligand σ-bonding destabilization of the singly occupied highest occupied molecular orbital (HOMO) of copper(II) in complexes with alternating fused 5-6-5 chelate rings compared to those with 5-5-5 chelate rings. Values close to 90° for the angles around copper provide a better orientation of the nitrogen electron pairs and bonds in the former case, as discussed above. The slight distortion of the planar environment of the copper(II) ion found in $[CuL^2]^{2-}$ would account for the small blue shift in its visible spectrum compared to that of $[CuL^3]^{2-}$. Not only the structure and spectroscopic properties of this family of copper(II) complexes are influenced by the specific ligand substitution pattern, but also their electrochemical behavior will depend on the ring size afforded by the polychelating ligand, as is discussed later.

The electronic absorption spectrum of the electrochemically generated copper(III)–L^3 complex in acetonitrile is also shown in Fig. 5, and compared to that of the corresponding copper(II) complex **7** [curves (*d*) and (*c*), respectively]. Three relatively intense bands are observed: two at 370 and 540 nm, with a third one in the form of a weak shoulder at 435 nm. The high-energy and more intense band in the spectrum of this copper(II) species is often charge transfer in origin (LMCT).[9] The low-energy single band [also observed in the spectrum of the copper(II) complex as a single band with almost the same location but significantly lower intensity] accounts for its deep purple color and would be a d–d transition band. However, since the L^3 ligand is innocent in the sense discussed above, all these bands may originate from d–d transitions. Three transitions are

‡ The visible spectra in acetonitrile are identical to those in dichloromethane which is generally regarded as a non-co-ordinating solvent, indicating thus that there is no significant axial co-ordination of acetonitrile to the copper(II) species in solution. By contrast, the visible absorption maxima in aqueous solution are significantly shifted to higher wavenumbers (590–570 nm). This shift of the $Cu^{II}L^n$ complexes is accompanied by a dramatic change of color, *i.e.* from red to deep blue ($n = 3$), purple to green ($n = 2$) and violet to light blue ($n = 1$). These spectral features clearly indicate a lowering of the tetragonal distortion for each copper(II) complex as a result of axial water co-ordination.

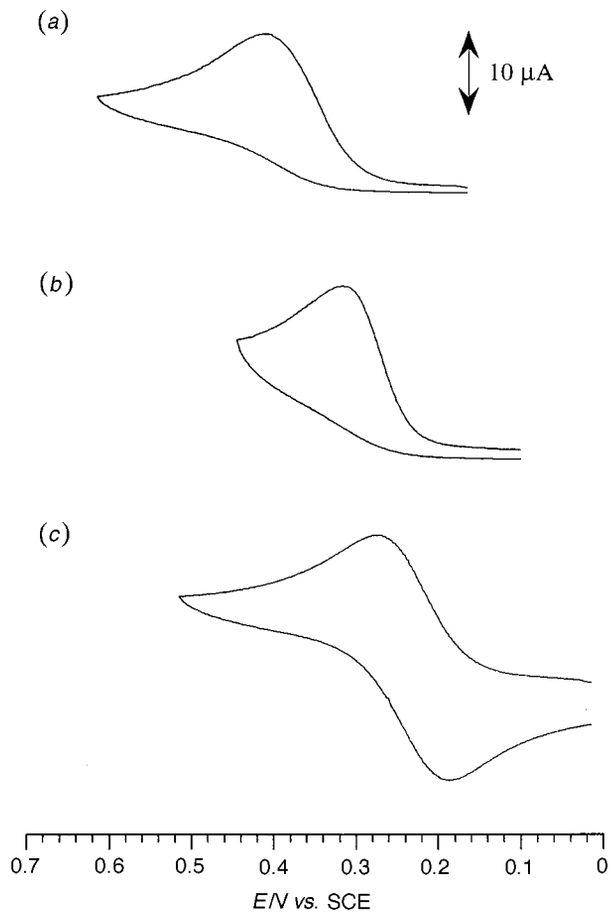

Fig. 6 Cyclic voltammograms of the copper(II) complexes **1** (*a*), **4** (*b*) and **7** (*c*) in acetonitrile at 100 mV s^{-1}

expected for a diamagnetic copper(III) ion with a d^8 electronic configuration in square-planar environment. They correspond to the individual transitions from the four lower-lying fully occupied d orbitals to the upper empty d orbital (*i.e.* $^1A_{1g} \longrightarrow {}^1B_{1g}$, $^1A_{1g} \longrightarrow {}^1A_{2g}$ and $^1A_{1g} \longrightarrow {}^1E_{1g}$ in ideal D_{4h} symmetry).[1] This upper orbital is $d_{x^2-y^2}$ (b_{1g}), where the *x* and *y* axes are defined by the metal–ligand bonds. Generally, if the crystal-field strength in the square-planar configuration is very high and only σ bonding is involved, as is the case for the L^3 ligand, the d_{z^2} (a_{1g}) orbital would be the low-lying orbital. Then, the high-energy UV band in the electronic absorption spectrum of the $[CuL^3]^-$ complex can be assigned to the $^1A_{1g} \longrightarrow {}^1B_{1g}$ transition. Furthermore, the intensity of this $\sigma \longrightarrow \sigma^*$ transition is expected to be much greater than any of the other $\pi \longrightarrow \sigma^*$ transitions, as is experimentally found. It is not possible to determine unequivocally the assignment of the two transitions within this latter group because the energy order of the d_{yz},d_{zx} (e_g) and d_{xy} (b_{2g}) orbitals of π symmetry is unknown. Nevertheless, the lowest transition which is associated with the low-energy visible band in the electronic absorption spectrum of the $[CuL^3]^-$ complex is probably the $^1A_{1g} \longrightarrow {}^1A_{2g}$, and, consequently, the shoulder on the low-energy tail of the high-energy UV band would correspond to the $^1A_{1g} \longrightarrow {}^1E_{1g}$ transition.

Electrochemical study

The electrochemical behavior of this series of copper compounds is illustrated in Fig. 6, which shows the voltammograms of **1**, **4** and **7** in acetonitrile at a scan rate of 100 mV s^{-1} [curves (*a*)–(*c*), respectively]. All the complexes exhibit an oxidation peak in the narrow potential range 0.41–0.27 V *vs.* SCE. If the sweep is reversed immediately after this peak the corresponding reduction peak is detected only for **7**, thus revealing that a fast

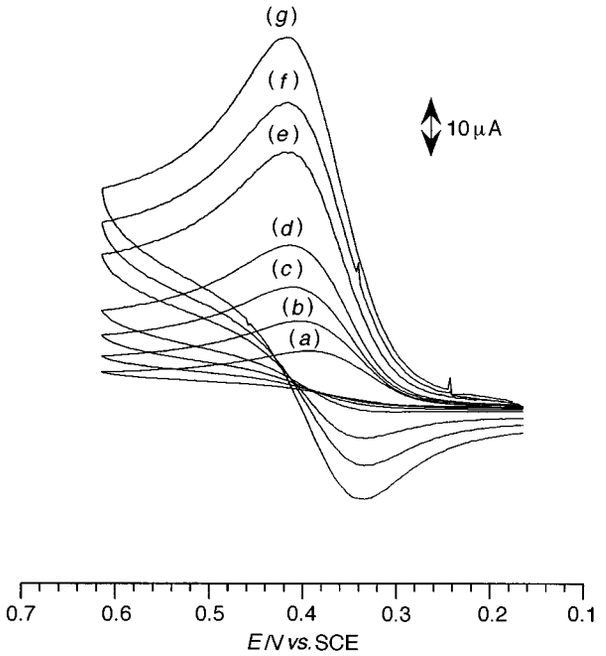

Fig. 7 Cyclic voltammograms of complex **1** in acetonitrile at different scan rates [(*a*) 20, (*b*) 50, (*c*) 100, (*d*) 200, (*e*) 500, (*f*) 750 and (*g*) 1000 mV s^{-1}]

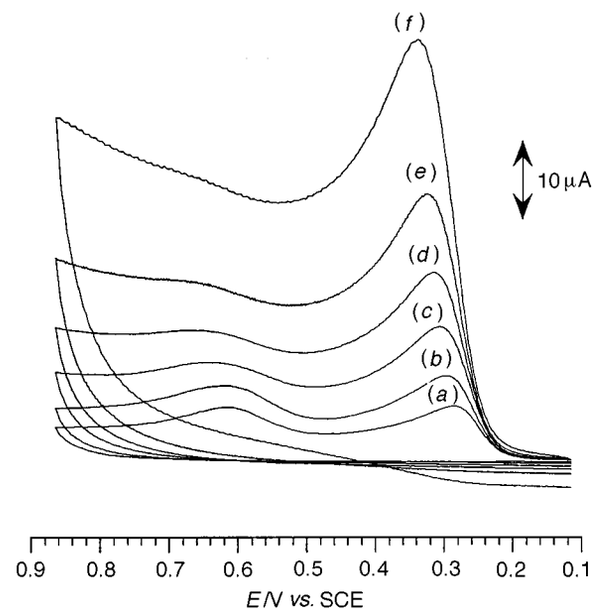

Fig. 8 Cyclic voltammograms of complex **4** in acetonitrile at different scan rates [(*a*) 10, (*b*) 20, (*c*) 50, (*d*) 100, (*e*) 200 and (*f*) 500 mV s^{-1}]

chemical reaction is coupled to the electrochemical process for both **1** and **4**. At the time[1] this decomposition reaction observed for $[CuL^1]^-$ was attributed to hydrolysis of the secondary amides from the oxamate ligand L^1 catalyzed by the trivalent copper, yielding oxalate and the aromatic diamine as final products (or their corresponding copper complexes). A reverse reduction peak is detected at scan rates higher than 200 mV s^{-1} (Fig. 7) for the oxidation of **1**, which is not observed for **4** even at the highest scan rate available. A second oxidation peak of lower intensity is observed after the first one for **4**, *i.e.* around 0.66 V *vs.* SCE. Its intensity increases as the scan rate decreases (Fig. 8), which unambiguously indicates that it corresponds to a redox process of a decomposition product. A similar copper(III)-catalyzed hydrolytic reaction should then be operative for complexes $[CuL^1]^-$ and $[CuL^2]^-$. The slight differences between their electrochemical behavior can be rationalized on a structural basis: the greater deviation from planarity for the oxamate ligand in $[CuL^2]^-$ compared to that in $[CuL^1]^-$, as discussed above, leads to a decrease in conjugation and consequently facilitates hydrolysis of the amido groups. For a family of *N*,*N*′-bis(carboxylate substituted)oxamide ligands related to those used herein, some of us have previously shown that the copper(III)-assisted hydrolysis of the oxamidate ligand can be analyzed in terms of the lack of planarity of the oxamidate ligand induced by the steric effect of the amide substituent.[10]

It should be noted that the above explanation was based on the principal assumption that the oxidation of each copper(II) complex is a metal-centered process. The observation that the oxidized species $[CuL^3]^-$ is stabilized toward decomposition relative to $[CuL^2]^-$ on the time-scale of the cyclic voltammetry experiments further supports this idea. Aliphatic amides are more reluctant to undergo hydrolysis than aromatic amides. Since alkyl groups are electron donating owing to their well known inductive donating effects, replacement of a naphthalene by a trimethylene residue decreases the positive charge density on the amide carbon and, hence, decreases its susceptibility to nucleophilic attack by H_2O. The peak-to-peak separation ΔE of the copper(III)–copper(II) couple of **7** for which both anodic and cathodic peaks were detected is similar to that of the ferrocenium–ferrocene couple under the same conditions, *i.e.* 80 mV. Furthermore, a linear plot of the peak current *vs.* the square root of the scan rate was obtained for that couple (Fig. 9), which is then stated to be reversible. However, the fact that the electrochemically generated $[CuL^3]^-$ complex is not indefinitely stable in acetonitrile is probably due to the occurrence of the copper(III)-promoted hydrolytic reaction also in that case.§ In fact, a change of color from deep purple to light brown occurs when allowing the solution to warm to room temperature, indicating decomposition of this unstable copper(III) species. This is accompanied by fading of the two more intense bands in the electronic absorption spectrum of the $[CuL^3]^-$ complex.

The trend in the formal potentials in acetonitrile solution of the Cu^{III}–Cu^{II} couple which occurs upon ligand substitution along this series of copper(II) complexes can also be accounted by assuming that all the oxidized species are copper(III) complexes. A comparison of the redox potentials of the $[CuL^1]^{-/2-}$ and $[CuL^2]^{-/2-}$ couples, where both ligands L^1 and L^2 have the same set of donor atoms but differ in the size of the central chelating ring, shows that the copper(III) complex $[CuL^2]^-$ is much more stable (thermodynamically but not kinetically, as discussed above), *i.e.* the Cu^{III}–Cu^{II} potential is lowered by 100 mV (0.31 *vs.* 0.41 V). It should be noted that the energy of the visible absorption maximum for the copper(II) complex

§ The corresponding sodium salt **5** oxidizes in a completely irreversible manner with water as solvent and 0.1 mol dm^{-3} $NaNO_3$ as supporting electrolyte.[10] Furthermore, the shift to a more positive potential by *ca.* 70 mV of the Cu^{III}–Cu^{II} redox couple in aqueous solution (0.97 V) relative to acetonitrile (0.27 V) suggests that axial water co-ordination to the copper(II) species $[CuL^3]^{2-}$ is involved, as revealed by the shift of its visible absorption maximum in each solvent, *e.g.* that of the tetraphenylphosphonium salt **7** shifts from 535 nm in acetonitrile to 570 nm for the corresponding sodium salt **5** in water. It has been reported that the co-ordination of water to copper(II) polypeptide complexes increases the formal potential owing to the fact that copper(III) with a low-spin d^8 electronic configuration prefers square-planar co-ordination and has little affinity for axial ligands.[11] Thus, a greater gain in CFSE is expected for the Cu^{II}–Cu^{III} redox change in a square-planar copper(II) environment with respect to an octahedral one. The change from octahedral d^9 Cu^{II} to square-planar low-spin d^8 Cu^{III} involves a stabilization in terms of CFSE of 152/12 *Dq*, a somewhat smaller energy gain compared to that of the same process but keeping the square-planar stereochemistry (162/12 *Dq*). This change in formal potential presumably results also from complexation of the sodium ion by the copper complex anions through the oxygen atoms of each oxamato group, causing a weakening of the ligand field, and hence a decrease in the value of *Dq*. A similar phenomenon has been observed for a related class of amidoalkoxo copper compounds.[2e]

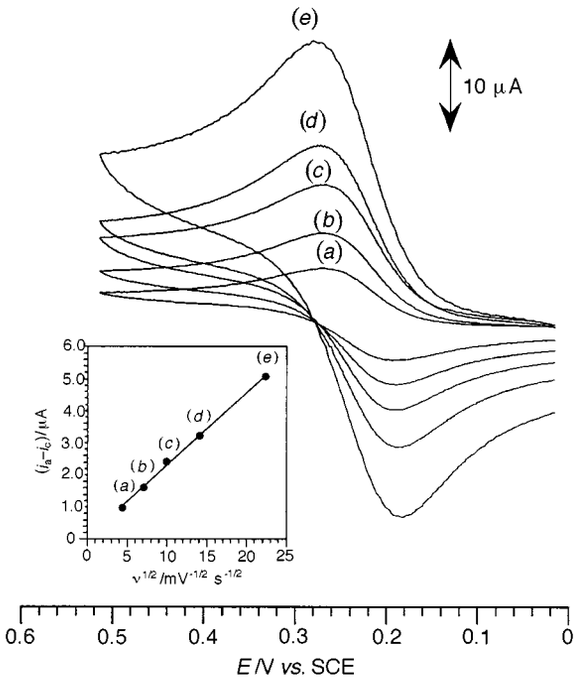

Fig. 9 Cyclic voltammograms of complex **7** in acetonitrile at different scan rates [(*a*) 20, (*b*) 50, (*c*) 100, (*d*) 200, (*e*) 500 mV s^{-1}]

$[CuL^2]^{2-}$ is higher than that of $[CuL^1]^{2-}$, thus suggesting that this chelate ring-size effect on the redox potential merely reflects the relative gain in the CFSE for the change from five- to six-membered chelate rings. In the case of the copper(III) ion which is expected to form more stable complexes than copper(II), this ligand-field effect of the chelate ring size becomes more important and, therefore, results in the observed shift of the formal potentials of the copper(III)–copper(II) couple.

We cannot definitely establish that the oxidation of both copper(II) complexes is metal centered. It would be possible for the oxidation of $[CuL^1]^-$ to be ligand centered, and for the substitution of the phenylene by the naphthalene fragment in $[CuL^2]^{2-}$ to cause a large enough increase in aromatic character to produce the observed negative shift in the formal potential. However, given that the diethyl ester derivative of the H_4L^2 ligand oxidizes at a potential much more positive than that of the copper(II) complex $[CuL^2]^{2-}$ (1.55 V), and even the diethyl ester derivative of H_4L^1 shows no tendency to oxidize below 1.80 V, it is most likely that the oxidation of both $[CuL^1]^{2-}$ and $[CuL^1]^{2-}$ is metal centered. The differences in the electrochemical behavior of the two ligands are related to the higher aromaticity of H_4L^2 compared to H_4L^1, as mentioned above. On the other hand, if the oxidation of $[CuL^2]^{2-}$ mainly involves the aromatic fragment of the ligand L^2, then the replacement of the naphthalene by the trimethylene bridge (complex $[CuL^3]^{2-}$) would result in an increase of the formal potential. However, the formal potential decreases by 40 mV (0.27 V) revealing that the higher oxidation state is stabilized. The stronger basicity of the aliphatic amido groups (electron-donor character) compared to the aromatic amido ones (electron-withdrawing character) accounts for this fact. Once again, this small negative shift of the Cu^{III}–Cu^{II} potential is consistent with the small difference in energies of the visible absorption maxima for the corresponding copper(II) complexes $[CuL^2]^{2-}$ and $[CuL^3]^{2-}$, which also suggests that a similar distortion of the planar environment of the metal ion would be operative for the copper(III) complex $[CuL^2]^-$. The relationship between redox potentials and visible absorption maxima has previously been demonstrated by us for the related family of disubstituted oxamide ligands derived from the parent *N*,*N*′-*o*-phenylenebis(oxamate) (L^1), namely its methylamide (L^5) and bis(methylamide) (L^6) derivatives.[1] This is nicely illustrated in

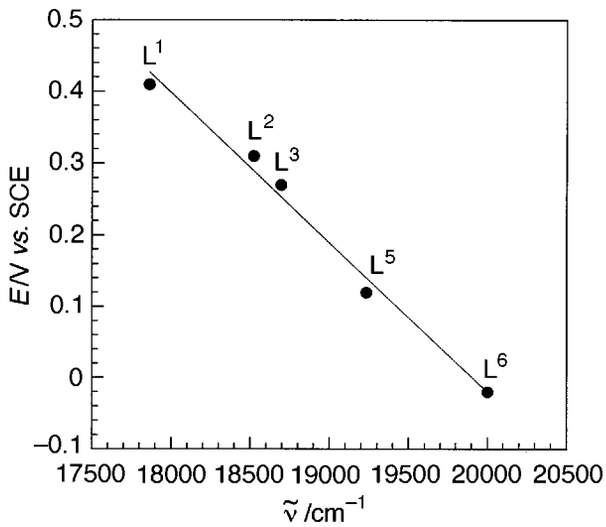

Fig. 10 Plot of the Cu^{III}–Cu^{II} redox potential (*vs.* SCE) against the copper(II) d–d absorption maxima for copper complexes with substituted oxamate and oxamide ligands

Table 6 The Cu^{III}–Cu^{II} redox potentials (*vs.* SCE) for copper complexes of a related class of substituted oxamate and oxamide ligands

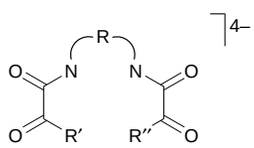

R	R′	R″	Ligand	*E*/V (Δ*E*/mV)
	O	O	L^1	0.41 *
	O	NMe	L^5	0.12 (50)
	NMe	NMe	L^6	−0.02 (50)
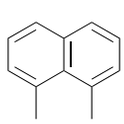	O	O	L^2	0.31 *
	O	O	L^3	0.27 (80)

* Irreversible couple.

Fig. 10. A linear correlation exists between the Cu^{III}–Cu^{II} redox potential and the copper(II) d–d absorption maxima over a range of potentials of 430 mV and wavenumbers of about 2000 cm^{-1}, indicating that the electronic and redox properties of this series of copper(II) complexes are intimately related. The relative gain in CFSE from the d^9 (Cu^{II}, square planar) to the low-spin d^8 (Cu^{III}, square planar) electronic configuration is the main factor in the overall thermodynamic stability of the copper(III) complexes and, consequently, oxidation occurs unambiguously at the metal center.

In summary, this and earlier work [1] on the copper chemistry of a related class of substituted oxamate and oxamide ligands confirms that the systematic changes in the ligand design (*e.g.* variation in the donor-atom set, conformational rigidity or flexibility, and/or the chelate ring sizes) are clearly reflected in the stabilization of high-oxidation-state copper(III) complexes, as indicated by the values of the corresponding Cu^{III}–Cu^{II} redox potentials summarized in Table 6. In continuing our studies on the redox chemistry of this series of copper compounds we have been able to identify the copper(III)-promoted amide hydrolysis as the main process accounting for the kinetic instability of the copper(III) complexes towards ligand degrad-

ation. We have demonstrated that it is possible to slow down or completely block these undesirable decomposition processes by adjusting the electron-donor character of the amide substituents. It is noteworthy that inclusion of alkyl substituents into the amide groups efficiently protects them from hydrolysis as evidenced by the L^6 ligand (see Table 6) with which we succeeded in preparing a stable copper(III) complex.[1] Our results on the co-ordination chemistry of oxamato- and oxamidatocopper(III) complexes complements pioneering studies by Margerum[12] (tri- and tetra-peptide complexes) and Fabbrizzi[13] (cyclam and dioxocyclamato complexes) and subsequently by Collins and their co-workers[2e] (amidophenoxo and amidoalkoxo complexes). These works and the present one clearly shows that Cu^{III} can no longer be considered a rare oxidation state.

Acknowledgements

We thank Dr. I. Fernández for recording the ^1H NMR spectra. Financial support from the Dirección General de Investigación Científica y Técnica (DGICYT) (Spain) through Project PB94-1002 is gratefully acknowledged. R. R. and B. C. thank the Ministerio de Educación y Ciencia (Spain) and the Conselleria de Educació i Ciència de la Generalitat Valenciana (Spain) for post- and pre-doctoral grants, respectively.

References

1 R. Ruiz, C. Surville-Barland, A. Aukauloo, E. Anxolabehere-Mallart, Y. Journaux, J. Cano and M. C. Muñoz, *J. Chem. Soc., Dalton Trans.*, 1997, 745.
2 (*a*) P. J. M. W. L. Birker, *J. Chem. Soc., Chem. Commun.*, 1977, 444; (*b*) W. E. Keys, J. B. R. Dunn and T. M. J. Loehr, *J. Am. Chem. Soc.*, 1977, **99**, 4527; (*c*) K. J. Oliver and T. N. Waters, *J. Chem. Soc., Chem. Commun.*, 1982, 1111; (*d*) L. L. Diaddario, W. R. Robinson and D. W. Margerum, *Inorg. Chem.*, 1983, **22**, 1021; (*e*) F. C. Anson, T. J. Collins, T. G. Richmond, B. D. Santarsiero, J. E. Toth and B. G. R. T. Treco, *J. Am. Chem. Soc.*, 1987, **109**, 2974 and refs. therein; (*f*) B. R. Serr, C. E. L. Headford, C. M. Elliot and O. P. Anderson, *Acta Crystallogr., Sect. C*, 1990, **46**, 500; (*g*) M. R. Caira, K. R. Koch and C. Sacht, *Acta Crystallogr., Sect. C*, 1991, **47**, 26; (*h*) T. M. Yao, X. Z. You, C. Li, L. F. Li and Q. C. Yang, *Acta Crystallogr., Sect. C*, 1994, **50**, 67; (*i*) J. Hanss and H. J. Krüger, *Angew. Chem., Int. Ed. Engl.*, 1996, **35**, 2827.
3 H. O. Stumpf, Y. Pei, O. Kahn, J. Sletten and J. P. Renard, *J. Am. Chem. Soc.*, 1993, **115**, 6738.
4 K. Nonoyama, H. Ojima and M. Nonoyama, *Inorg. Chim. Acta*, 1976, **20**, 127.
5 G. M. Sheldrick, SHELXS 86, A Program for Crystal Structure Determination, University of Göttingen, 1986; SHELXL 93, Program for the Refinement of Crystal Structures, University of Göttingen, 1993.
6 *International Tables for X-Ray Crystallography*, Kynoch Press, Birmingham, 1974, vol. 4, p. 99.
7 C. K. Johnson, ORTEP, Report ORNL-3794, Oak Ridge National Laboratory, Oak Ridge, TN, 1971.
8 S. S. Turner, C. Michaut, O. Kahn, L. Ouahab, A. Lecas and E. Amouyal, *New J. Chem.*, 1995, **19**, 773.
9 A. W. Hamburg and D. W. Margerum, *Inorg. Chem.*, 1983, **22**, 3884.
10 J. Soto, R. Martínez-Máñez, J. Payá, F. LLoret and M. Julve, *Transition Met. Chem.*, 1993, **18**, 69.
11 M. P. Youngblood and D. W. Margerum, *Inorg. Chem.*, 1980, **19**, 3068.
12 D. W. Margerum, K. L. Chellapa, F. P. Bossu and G. L. Burce, *J. Am. Chem. Soc.*, 1975, **97**, 6894; (*b*) F. P. Bossu, K. L. Chellapa and D. W. Margerum, *J. Am. Chem. Soc.*, 1977, **99**, 2195.
13 L. Fabbrizzi, A. Perotti and A. Poggi, *J. Chem. Soc., Chem. Commun.*, 1980, 646; (*b*) L. Fabbrizzi and A. Poggi, *Inorg. Chem.*, 1983, **22**, 1411.

Received 26*th September* 1997; *Paper* 7/06964B